The Astrophysical Journal, 906:10 (9pp), 2021 January 1 https://doi.org/10.3847/1538-4357/abc5b1

Investigating the Mini and Giant Radio Flare Episodes of Cygnus X-3

Elise Egron[1], Alberto Pellizzoni[1], Simona Righini[2], Marcello Giroletti[2], Karri Koljonen[3,4], Katja Pottschmidt[5,6], Sergei Trushkin[7,8], Jessica Lobina[9], Maura Pilia[1], Joern Wilms[10], Stéphane Corbel[11,12], Victoria Grinberg[13], Sara Loru[14], Alessio Trois[1], Jérome Rodriguez[11], A. Lähteenmäki[4,15], M. Tornikoski[4], S. Enestam[4], and E. Järvelä[4]

[1] INAF-Osservatorio Astronomico di Cagliari, Via della Scienza 5, I-09047 Selargius, Italy; elise.egron@inaf.it
[2] INAF, Istituto di Radio Astronomia di Bologna, Via P. Gobetti 101, I-40129 Bologna, Italy
[3] Finnish Centre for Astronomy with ESO (FINCA), University of Turku, Väisäläntie 20, FI-21500 Piikkiö, Finland
[4] Aalto University Metsähovi Radio Observatory, Metsähovintie 114, FI-02540, Kylmälä, Finland
[5] CRESST and NASA Goddard Space Flight Center, Astrophysics Science Division Code 661, Greenbelt, MD 20771, USA
[6] Center for Space Science and Technology, University of Maryland Baltimore County, 1000 Hilltop Circle, Baltimore, MD 21250, USA
[7] Special Astrophysical Observatory of the Russian Academy of Sciences, Niznij Arkhyz 369167, Russia
[8] Kazan Federal University, Kazan, 420008, Russia
[9] Dipartimento di Fisica, Università degli Studi di Cagliari, SP Monserrato-Sestu, KM 0.7, I-09042 Monserrato, Italy
[10] Dr. Karl-Remeis-Sternwarte and Erlangen Centre for Astroparticle Physics (ECAP), Friedrich Alexander Universität Erlangen-Nürnberg, Sternwartstr. 7, D-96049 Bamberg, Germany
[11] Lab AIM, CEA/CNRS/Université Paris-Saclay, Université de Paris, F-91191 Gif-sur-Yvette, France
[12] Station de Radioastronomie de Nançay, Observatoire de Paris, PSL Research University, CNRS, Univ. Orléans, F-18330 Nançay, France
[13] Institut für Astronomie und Astrophysik, Universität Tübingen, Sand 1, D-72076 Tübingen, Germany
[14] INAF-Osservatorio Astrofisico di Catania, Via S.Sofia 78, I-95123 Catania, Italy
[15] Aalto University Department of Electronics and Nanoengineering, P.O. BOX 15500, FI-00076 AALTO, Finland
Received 2019 December 20; revised 2020 October 21; accepted 2020 October 26; published 2020 December 29

Abstract

The microquasar Cygnus X-3 underwent a giant radio flare in 2017 April, reaching a maximum flux of ∼16.5 Jy at 8.5 GHz. We present results from a long monitoring campaign carried out with Medicina at 8.5, 18.6, and 24.1 GHz, parallel to the Metsähovi radio telescope at 37 GHz, from 2017 April 4 to 11. We observe a spectral steepening from $\alpha = 0.2$ to 0.5 (with $S_\nu \propto \nu^{-\alpha}$) within 6 hr of the epoch of the flare's peak maximum, and rapid changes in the spectral slope in the following days during brief enhanced emission episodes while the general trend of the radio flux density indicated the decay of the giant flare. We further study the radio orbital modulation of Cyg X-3 emission associated with the 2017 giant flare and with six mini-flares observed in 1983, 1985, 1994, 1995, 2002, and 2016. The enhanced emission episodes observed during the decline of the giant flare at 8.5 GHz coincide with the orbital phase $\phi \sim 0.5$ (orbital inferior conjunction). On the other hand, the light curves of the mini-flares observed at 15–22 GHz peak at $\phi \sim 0$, except for the 2016 light curve, which is shifted 0.5 w.r.t. the other ones. We attribute the apparent phase shift to the variable location of the emitting region along the bent jet. This might be explained by the different accretion states of the flaring episodes (the 2016 mini-flare occurred in the hypersoft X-ray state).

Unified Astronomy Thesaurus concepts: High mass x-ray binary stars (733); Radio jets (1347)

Supporting material: data behind figure

1. Introduction

Discovered in 1966 (Giacconi et al. 1967), Cygnus X-3 is a unique and enigmatic X-ray binary system that consists of a low-mass compact object ($M \sim 2.4^{+2.1}_{-1.1}\,M_\odot$; Zdziarski et al. 2013) and a Wolf–Rayet star (van Kerkwijk et al. 1992, 1996; Koljonen & Maccarone 2018). The exact nature of the compact object is still unknown, but a black hole is favored according to its X-ray and radio properties (Hjalmarsdotter et al. 2008, 2009; Szostek et al. 2008; Koljonen et al. 2010). Contrary to other high-mass X-ray binaries (HMXBs), Cyg X-3 has a very short binary period $P_{\rm orb} \sim 4.8$ hr, which implies a very tight orbit ($\sim 3 \times 10^{11}$ cm) and strong interactions between the compact object and the Wolf–Rayet wind ($\dot{M} \sim 10^{-5}\ M_\odot\,{\rm yr}^{-1}$, $v_{\rm wind} \sim 1000\,{\rm km\,s^{-1}}$; van Kerkwijk et al. 1996; Koljonen & Maccarone 2018). The compact object appears to be totally enshrouded in the wind of the donor star.

Located in the Galactic plane at a distance of ∼7.4 ± 1.1 kpc (McCollough et al. 2016), Cyg X-3 is the brightest microquasar at radio wavelengths. Although it is in the quiescent state (∼100 mJy) most of the time, Cyg X-3 is characterized by a highly variable radio emission spanning from 1 to 30 mJy in the quenched radio state (Waltman et al. 1996) up to 20 Jy during the flaring states (Waltman et al. 1995; Mioduszewski et al. 2001; Miller-Jones et al. 2004; Corbel et al. 2012). Differently from what is observed in other microquasars, singular giant radio flares correspond to the transition from the ultra-soft X-ray state (the so-called hypersoft state; Szostek et al. 2008; Koljonen et al. 2010, 2018) to a harder state. The hypersoft state corresponds to unusual very soft X-ray spectra, associated with a quenched radio emission during which there is no or very faint radio emission that can last several weeks preceding the giant radio flare. The rise of the giant flares usually lasts for about 3 days while the decay is visible over ∼10–30 days (Trushkin et al. 2017). Relativistic jets are clearly resolved during these episodes using the Very Large Array (VLA), the Very Long Baseline Array (VLBA), and the European Very Long Baseline Interferometry Network (e-EVN; Martí et al. 2001; Mioduszewski et al. 2001; Miller-Jones et al. 2004; Tudose et al. 2007). Mini-flares were detected during the quiescent and quenched radio states. They are characterized by low-flux

amplitudes (up to 1 Jy) and have a duration of less than a day (Waltman et al. 1994). They are most likely associated with the compact jet emission (Newell et al. 1998; Egron et al. 2017).

A flux modulation, taken to represent the orbital period of the binary system, was first observed in the X-rays (Parsignault et al. 1972; Canizares et al. 1973) and subsequently in the infrared (Becklin et al. 1973). The X-ray minima occur at the superior conjunction, when the compact object lies behind the Wolf–Rayet star. The X-ray modulation depth decreases with increasing energy above 5 keV, which is interpreted as bound-free absorption and Compton scattering in the stellar wind of the donor (Zdziarski et al. 2012). In this scenario, the X-ray minima correspond to the highest optical depth at the superior conjunction. A decrease of the optical depth below 3 keV is instead attributed to the re-emission of the absorbed continuum by the wind in soft X-ray lines (Zdziarski et al. 2012). The X-ray orbital period increases with time ($\dot{P}/P \sim 1 \times 10^{-6}$ yr^{-1}; van der Klis & Bonnet-Bidaud 1981; Kitamoto et al. 1987, 1995; Singh et al. 2002). This slow-down is ascribed to the loss of angular momentum through the mass loss of the stellar wind (Davidsen & Ostriker 1974).

Cyg X-3 was the first microquasar detected in the gamma rays above 100 MeV with Fermi/LAT and AGILE (Fermi LAT Collaboration et al. 2009; Tavani et al. 2009). Inverse-Compton scattering of soft photons from the Wolf–Rayet companion on relativistic electrons in the jet naturally explains the gamma-ray emission (Dubus et al. 2010). This high-energy emission is associated with transitions into and out of the quenched radio state, probably due to shocks forming at various distances along the jet (Corbel et al. 2012; Koljonen et al. 2018). Bright gamma-ray emission is also detected during the mini-flares, when shocks occur closer to the core of the jet, hence deeper in the Wolf–Rayet wind. The gamma-ray emission was found to be strongly modulated at the orbital period of the system (Fermi LAT Collaboration et al. 2009; Zdziarski et al. 2018), but shifted by a half orbital period with respect to the X-ray modulation. A jet inclination of $\sim 30^{\circ}$ with respect to the orbital plane is required in order to obtain good fits to the gamma-ray modulation (Dubus et al. 2010; Zdziarski et al. 2018). An inclined jet is likely to undergo precession and strongly affect the gamma-ray modulation shape at different epochs. However, there is currently no evidence for such a jet precession in gamma rays. Instead, a jet precession was clearly detected during giant radio flares at much larger distances from the compact object (Mioduszewski et al. 2001; Miller-Jones et al. 2004).

A modulation of the radio flux at the orbital period has been claimed in the HMXB Cyg X-1 (Fender et al. 1997b; Pooley et al. 1999). This variable absorption of the flux density has been attributed to the stellar wind, as the black hole jet orbits around the OB companion star (Brocksopp et al. 2002; Szostek & Zdziarski 2007). A similar orbital modulation was also expected in Cyg X-3. A 4.8 hr orbital modulation has been highlighted at radio wavelengths during low-level radio flares from Cyg X-3 (Molnar et al. 1984), but no orbital modulation was later confirmed. A pronounced modulation of the radio emission has been recently detected by Zdziarski et al. (2018), who performed a careful study of the archival radio emission at 15 GHz. The amplitude of the modulation is found to depend on both the X-ray spectral state and the radio flux, changing from 2.5% to 10%. The radio orbital modulation is well modeled by free–free absorption by the stellar wind.

VLBI observations performed at 22 GHz during the 2016 mini-flare showed a short timescale variability, with evidence of two peaks at different flux densities (Egron et al. 2017). At a first glance, the difference between the two peaks corresponds to the orbital period of Cyg X-3. In order to investigate possible orbital modulation effects during mini-flare events, we collected previous mini-flare observations (above 100 mJy and below 1 Jy; Waltman et al. 1996) carried out at 15 and 22 GHz with interferometric antennas. The motivation for using such observations is their duration (usually several continuous hours), which is of utmost importance to provide a dense flux coverage of at least a whole orbital period of the binary system. We excluded data at other frequencies since there are not enough sampled and therefore they are not suitable for a statistic analysis of light curves when considering them alone.

In this paper, we present the monitoring of the 2017 April giant flare carried out with the Medicina 32 m and the Metsähovi 13.7 m radio telescopes. We study the evolution of the radio flux and spectral index during this event. In the frame of the presently limited and sparse samples preventing an extensive orbital timing analysis, we provide evidence of radio orbital modulation during specific episodes of Cyg X-3, the giant flare, and mini flares, where the jet characteristics and morphologies are very different.

2. Radio Data

2.1. Medicina Multifrequency Observations during the 2017 Giant Flare

Following the detection of the start of the flare in Cyg X-3 by the RATAN (Trushkin et al. 2017), we triggered a Target-of-Opportunity program with the Medicina radio telescope (32 m; www.med.ira.inaf.it) in order to follow the evolution of the radio emission during the whole duration of the giant flare. The frequency agility offered by Medicina (i.e., the change of the observing receiver/frequency requiring at most a few minutes), allowed us to carry out observations at 8.5, 18.6, and 24.1 GHz (typically 30 minutes each) from 2017 April 4 to 11. These long sessions lasting from 3 to 11 hr per day were aimed at tracking possible changes in the radio spectral index. We performed on-the-fly cross-scans in RA and DEC directions, setting a bandwidth of 680 MHz. Scans were performed along a length of $0\overset{\circ}{.}6$, at a velocity of $2\overset{\prime}{.}4$ s at 8.5 GHz. We selected a bandwidth of 1200 MHz, scans of $0\overset{\circ}{.}2$ in length and a scan velocity of $0\overset{\prime}{.}8$ s in the K band (18.6 and 24.1 GHz). Data calibration was carried out through the observation of NGC 7027 at each frequency, within 1 hr of Cyg X-3 acquisitions. We extrapolated the calibrator flux density according to Ott et al. (1994): 5.764 ± 0.005 Jy at 8.5 GHz, 5.508 ± 0.009 Jy at 18.6 GHz, and 5.367 ± 0.015 Jy at 24.1 GHz.

The calibration procedure included the corrections for the frequency-dependent gain curves, plus the compensations for the pointing offset measured on each scan. Corrections for atmospheric opacity were applied to the K-band measurements only. In order to improve the accuracy of the flux density measurements, we carried out additional observations of the bright H II region DR21 ($F \sim 20$ Jy at 18.6 GHz) because of its location very close to Cyg X-3 (angular separation $\sim 1\overset{\circ}{.}8$). It allowed us to apply additional gain curve corrections, in particular at low elevations, where the standard curve is less

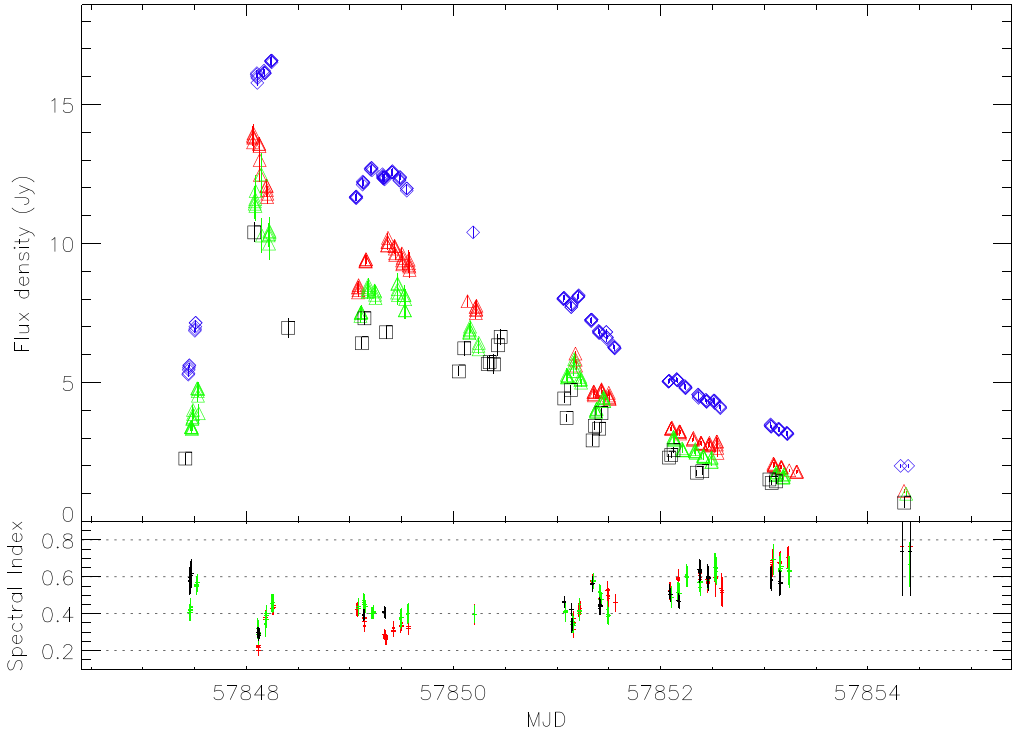

Figure 1. Top panel: Medicina observations performed at 8.5, 18.6, and 24.1 GHz (blue diamonds, red and green triangles, respectively) and MRO observations carried out at 37 GHz (black squares) during the giant flare from 2017 April 4 to 11. Bottom panel: evolution of the spectral index α between 8.5 and 18.6 GHz (red), between 8.5 and 24.1 GHz (green), and between 8.5 and 37 GHz (black).

(The data used to create this figure are available.)

effectual and is characterized by larger residuals. We rejected the *K*-band data acquired under unsuitable weather conditions (*K* band requires a uniform sky opacity as far as possible and no rain). We estimate the final accuracy of our measurements to be ∼5% in *K* band, while we obtain ∼3% errors at 8.5 GHz. The resulting light curve is presented in Figure 1 and the associated data are provided as data behind the Figure.

2.2. Metsähovi Radio Telescope Monitoring during the 2017 Giant Flare

With the onset of the Cyg X-3 outburst in 2017 April, we started monitoring observations with the 13.7 m diameter Metsähovi Radio Observatory (MRO) at 37 GHz. The observations were made in dual beam switching mode, alternating the source and the sky in each feed horn. A typical integration time to obtain one flux density data point was between 1200 and 1400 s. The detection limit of the telescope at 37 GHz is on the order of 0.2 Jy under optimal conditions. Data points with a signal-to-noise ratio <4 are handled as nondetections.

The flux density scale is set by observations of DR 21. Sources NGC 7027, 3C 274, and 3C 84 are used as secondary calibrators. A detailed description of the data reduction and analysis is given in Teräesranta et al. (1998). The error estimate in the flux density includes the contribution from the measurement rms and the uncertainty of the absolute calibration. The data are shown in Figure 1 together with the Medicina multifrequency observations, and the associated data are provided as data behind the Figure.

2.3. Interferometric Data during the Mini Flares

We used interferometric observations from the literature that contained mini-flare observations of Cyg X-3: VLA data from 1983 September 17–18 (Molnar et al. 1984), VLBI data from 1985 February 5 (Molnar et al. 1988), Ryle telescope data obtained on 1994 June 3 (Waltman et al. 1996), VLBA data from 1995 May 7 (Newell et al. 1998), Ryle telescope and VLA observations from 2002 January 25 (Miller-Jones et al. 2009), and more recently VLBI observations corresponding to the mini-flare observed a few days before the onset of the giant flare on 2016 September 1 (Egron et al. 2017).

VLA observations were carried out in A configuration on 1983 September 17 and 18 from 1:30 to 7:30 UT (both days) at 1.3, 2, 6, and 20 cm. For our study, we restricted our analysis to the 2 cm data (15 GHz). A composite array of five VLBI antennas was used to perform observations of Cyg X-3 at 22 GHz on 1985 February 5. Due to some telescope problems, only four antennas were employed during both sets of observations, which lasted for ∼7 hr. Observations of Cyg X-3 were carried out at 15 GHz with the Ryle telescope in 1994 and 1995, during gaps between the prime observing targets. The VLBA observations performed on 1995 May 7 from 08:40 to 17:45 UT were conducted at 15.3 GHz using all 10 antennas. The data were correlated at the VLBA correlator in Socorro, New Mexico. Cygnus X-3 was observed on 2002 January 25 for 8 hr with the VLA in A-configuration. The VLA was split into two subarrays in order to perform simultaneous observations at 14.94 GHz and at 43.34 GHz. The source was also observed at 15 GHz by the Ryle telescope, overlapping the VLA observations for 1.6 hr at the beginning of the VLA run. Recent VLBI observations were conducted on 2016 September

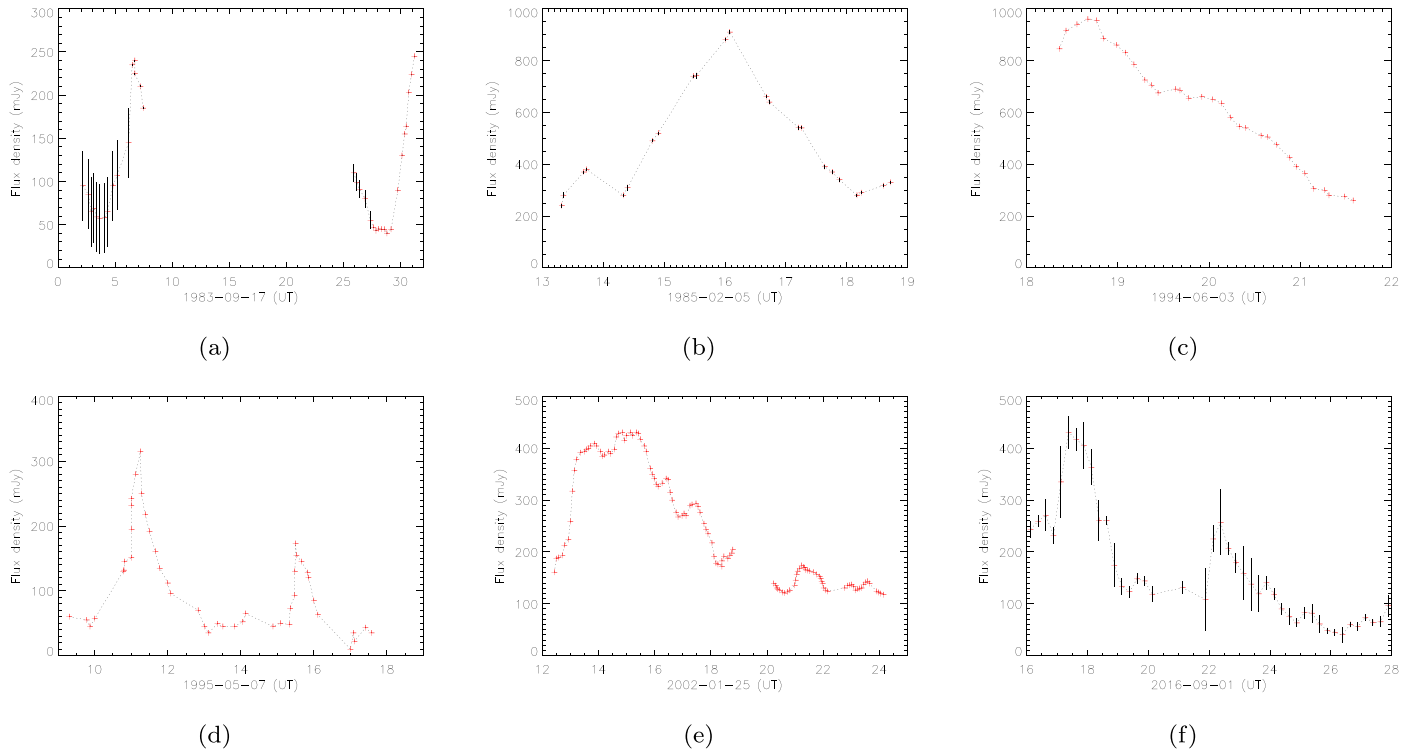

Figure 2. Light curves of Cyg X-3 obtained during mini-flares on (a) 1983 September 17–18 (MJD 45594, 45595) at 15 GHz (Molnar et al. 1984) with the VLA, (b) 1985 February 5 (MJD 46101) at 22 GHz (Molnar et al. 1988) with the VLBI, (c) 1994 June 3 (MJD 49506) at 15 GHz (Waltman et al. 1996) with the Ryle telescope, (d) 1995 May 7 (MJD 49844) at 15 GHz (Newell et al. 1998) with the VLBA, (e) 2002 January 25 (MJD 52299) at 15 GHz with the Ryle telescope and the VLA (Miller-Jones et al. 2009), and (f) 2016 September 1 (MJD 57632) at 22 GHz (Egron et al. 2017) with the VLBI.

1 at 22 GHz with the SRT (64 m, Italy), Medicina (32 m, Italy), Noto (32 m, Italy), Torun (32 m, Poland), Yebes (40 m, Spain), and Onsala (20 m, Sweden) for approximately 12 h. The data were processed with the DiFX correlator (Deller et al. 2011) installed and operated in Bologna, Italy.

We did not reanalyze the data, but used the resulting light curves presented in the different papers to perform our study. The associated light curves are shown in Figure 2.

3. The 2017 Giant Flare

Radio flares are caused by synchrotron radiation from accelerated relativistic electrons suffering radiative, adiabatic, and energy-dependent loss mechanisms. Particles can be accelerated in (1) discrete plasmoids evolving from optically thick to optically thin as they move outward from the core and quickly expand (van der Laan 1966; Hjellming & Johnston 1988; Atoyan & Aharonian 1999), (2) internal shocks in the jet (Fender et al. 2004; Lindfors et al. 2007; Miller-Jones et al. 2009), or (3) magnetic reconnection in the relativistic plasma with a relatively high magnetization (Guo et al. 2014; Sironi & Spitkovsky 2014; Sironi et al. 2016).

During the 2017 April giant flare, the flux density of Cyg X-3 increased expeditiously to reach a peak maximum of 16.6 $\pm$0.3 Jy at 8.5 GHz on April 5 (MJD 57848), as shown in Figure 1. The radio emission observed at 18.6, 24.1, and 37 GHz followed a similar trend apart from the 8.5 GHz flux density, which was still rising on April 5 while the flux were already weakening at higher frequencies. Figure 1 provides evidence of small and short-duration flux fluctuation at different frequencies during the general declining trend of the giant flare on April 6 and 8. A frequency-dependent slight delay between the different light curves has been observed for instance in Molnar et al. (1984, 1988). In our data, the above increases of flux density seem to appear first at higher frequency (37 GHz, then 24.1, 18.6, and 8.5 GHz), but the presence of a significant delay cannot be firmly confirmed due to the lack of perfectly simultaneous and continuous observations.

We studied the evolution of the spectral index α (with $S_\nu \propto \nu^{-\alpha}$) by considering all pairs of flux density measurements available at low (8.5 GHz) and high frequencies (18.6, 24.1, and 37 GHz) within 1 hr from each other. Spectral index errors were derived from error propagation of flux density errors for each pair. The time tag of the reported spectral index values corresponds to the mid time between the epochs of each flux density measurement pair. The error bars on the x-axis (time) reflect the epoch separation for each pair of flux density measurements. As shown in Figure 1, we observed a spectral steepening from $\alpha = 0.22 \pm 0.05$ to 0.45 ± 0.05 between 8.5 GHz and 18.6 GHz, and from $\alpha = 0.3 \pm 0.1$ to 0.46 ± 0.05 between 8.5 GHz and 24.1 GHz within $\sim$6 hr at the time of the peak maximum of the flare (April 5). The spectral index then continuously varied in the following days. In particular it flattened then steepened from $\alpha \sim 0.3$ to $\sim$0.4 on MJD 57849 and from $\alpha \sim 0.3$ to $\sim$0.6 on MJD 57851 when the radio flux density suddenly increased while the general trend indicated a flare decay. At the end of the giant flare ($F_{8.5\,\mathrm{GHz}} < 5$ Jy), the spectral index reached a value of $\sim$0.7.

Here, as well as in Egron et al. (2017), it has been shown that the radio spectral index varies in less than 6 hr at the time of the flare peak. The values of the spectral index are very similar to the ones associated with previous giant flares (Miller-Jones et al. 2004, and references therein). However, the long monitoring performed with Medicina during the 2017 giant

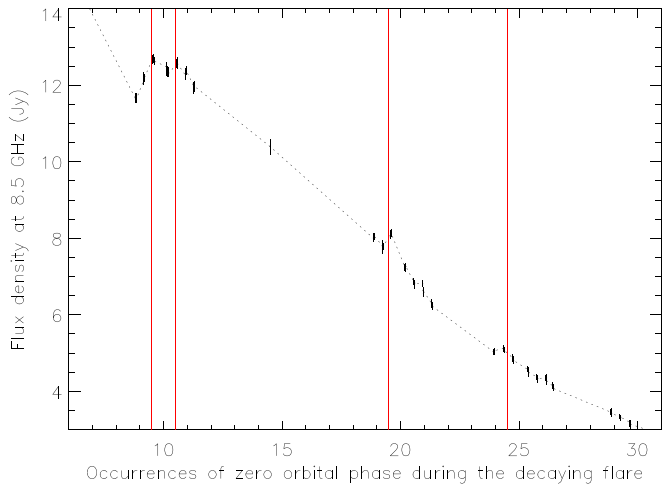

Figure 3. Medicina flux density at 8.5 GHz during the decaying giant flare in 2017 April as a function of the occurrences of zero orbital phase since the 84,621st orbital period of Cyg X-3. The vertical red lines highlight $\phi = 0.5$ corresponding to the most significant increases of flux density.

flare shows for the first time additional spectral variations (flattening then steepening) at the time of fast- and short-duration increases of flux density during the decaying flare.

4. Orbital Modulation

We searched for orbital modulation in the radio emission during the giant and mini-flare episodes, which are associated with extended and compact jets, respectively. A modulation of the radio emission from the jet is expected by variable free–free absorption in the wind from the companion star along the orbit (Molina et al. 2019). We considered the recent quadratic ephemeris from Bhargava et al. (2017), based on 45 yr of X-ray data obtained from the archives of the Einstein Observatory, EXOSAT, Ginga, and RXTE as well as the recent AstroSAT data:

$$T_n = T_0 + P_0 n + \frac{1}{2}\dot{P}P_0 n^2, \quad (1)$$

where $T_0 = 40949.384$ (MJD) is the epoch at the superior conjunction ($\phi = 0$), $P_0 = 0.19968476(3)$ days is the period at T_0, $\dot{P} = (5.42 \pm 0.02) \times 10^{-10}$ is the period derivative, and n is the orbit number. This recent ephemeris is based on barycenter-corrected X-ray light curves and given in Terrestrial Time MJD, as mentioned in Zdziarski et al. (2018).

4.1. Search for Orbital Modulation during the 2017 Giant Flare

Since the radio flux emission continuously changes during the 2017 giant flare on hour timescales, it would be speculative to provide a renormalization of the flux density to fold the light curve. Instead, we plotted the 8.5 GHz data, which are the most densely sampled measurements, as a function of the occurrences of zero orbital phases by applying ephemeris from Bhargava et al. (2017). Zero orbital phases refer to the X-ray minima at superior conjunction since MJD 40949.384, the T_0 references the epoch mentioned by Bhargava et al. (2017). Our first measurement at 8.5 GHz on MJD 57847.438 corresponds to the 84,621st orbital period of Cyg X-3. For clarity, we reported the occurrences of zero orbital phases since the 84,621th (Cyg X-3 performed about 38 orbital periods in ∼8 days). As shown in Figure 3, all four enhanced flux densities ranging from 2σ to 6σ during the decaying phase of the flare correspond to $\phi \sim 0.5$, which is aligned with the X-ray maxima. The corresponding amplitudes of the peaks range from 2.5% to 8% with respect to the general trend of the flare decay. On the other hand, about 50% of the available measurements at $\phi \sim 0.5$ does not show any significant flux enhancement. Thus, in order to confirm and quantify such a possible phase-flux correlation, a larger and denser monitoring at different frequencies would be required during the next giant flares of Cyg X-3.

4.2. Orbital Modulation during the Mini Flares

The light curve obtained during the 2016 mini flare shows the presence of two peaks of different intensity, separated by ∼4.8 hr (see Figure 2). The separation between these peaks apparently matches the orbital period of Cyg X-3. We therefore collected all available long and continuous archive observations of several hours obtained during mini-flare episodes to search for a possible orbital modulation during these events. Because mini-flares usually last less than a day and are not as predictable as giant flares are, only a few observations were carried out by chance.

Different observation programs based on interferometry were conducted in the 1980s in order to study the radio spectral evolution of Cyg X-3 in its low state (Molnar et al. 1984, 1988). Mini flares with a flux density <1 Jy were detected during these observations. The apparent flare separations near the 4.8 hr X-ray period suggests a direct correlation with the orbital period. Ten years later, subsequent observations were planned with the VLBA in order to investigate the jet structure during the quiescent state. Newell et al. (1998) observed two short-duration flares of ∼0.3 Jy and ∼0.13 Jy at 15.3 GHz on 1995 May 7 while the source was in the quiescent state for the rest of the observing run (see Figure 2). Here again, we note a peak separation of ∼4.8 hr. Thus, among the available data described above, all the data sets that present a clear double-peak signature also show a peak separation corresponding to the orbital period.

We computed the significance of a possible orbital period detection through simulations based on the generation of fake light curves with the same parameters of the observed data, but introducing random phase shifts for the light-curve peaks. Providing random double-peak distributions (10^8 trials), the combined probability of chance occurrence of peak separation at the orbital period related to the above double-peaked data sets is ∼0.02%, even assuming a conservative tolerance of 20 minutes. We then included in our statistical analysis the remaining data sets for which no double-peak distribution seems clearly present or it is not significant, assuming no detection for the latter. The cumulative chance probability (including all data trials) of having only the former data sets displaying a double-peak distribution at the orbital period is ∼0.15%. Thus, this preliminary analysis shows that our periodicity claim deserves detailed timing investigations being statistically significant at $>3\sigma$ level.

In order to investigate periodicities in the multiyear radio light curves of Cyg X-3, we phase-folded individual data sets at the system's orbital period using the X-ray ephemeris provided by Bhargava et al. (2017). Taking into account the number of available measurements, we could provide average flux density values for 12 orbital phase bins of 24 minutes each. In order to

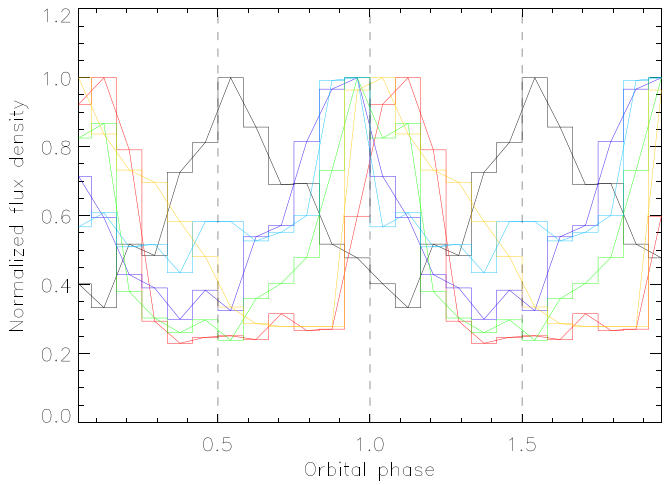

Figure 4. Phase-folded, renormalized light curves corresponding to the six mini-flare data sets (green: 1983, blue: 1985, orange: 1994, red: 1995, cyan: 2002, black: 2016), using ephemeris from Bhargava et al. (2017) and 12 bins. Phase 0 corresponds to the X-ray orbital phase 0 (superior conjunction).

ease the comparison among the different data sets, we normalized the folded light curves to their respective peak flux values (see Figure 4). The folded light curves related to 1983–2002 data are shifted of a half orbital period with respect to the X-ray maxima. Instead, the 2016 light-curve peaks in correspondence with the X-ray maxima ($\phi \sim 0.5 \pm 0.05$).

The orbital period is known with very good precision from X-ray observations ($P_0 = 0.19968476(3)$ days; Bhargava et al. 2017) and cannot be better constrained by the considered radio data set that includes only a few observed orbital revolutions. However, the phase folding of radio data could reveal a different localization of the bulk of the radio emission with respect to the X-ray emission. The jet emission associated with the 1995 and 1985 mini-flares is seen up to 2.0–2.5 mas (Molnar et al. 1988; Newell et al. 1998), while the 2016 mini-flare episode is resolved closer to the compact object (0.6–0.9 mas; Egron et al. 2017). Thus the interferometric observations revealed radio emission on the mas scale during mini-flare episodes, at distances much larger than the orbital separation ($\sim 3 \times 10^{11}$ cm) and the radius of the donor, which is expected to be less than the Roche lobe radius ($\sim 1.2 \times 10^{11}$cm; Zdziarski et al. 2018). This could require timing corrections related to the binary system geometry and emitting source motion during different flaring episodes.

Note that the location of the bulk emission and thus the amplitude modulation are most likely frequency-dependent, as observed in Cyg X-1 (Brocksopp et al. 2002; Zdziarski 2012). Since we jointly treated the orbital modulation at 15 and 22 GHz, the location of the two emissions during the same flare is expected to be slightly different along the jet.

Zdziarski et al. (2018) mentioned the presence of a pronounced peak in the power spectrum of the radio emission at $P_r = 0.19944848$ days, which is shorter by 20 s than the X-ray orbital period P_0. The authors associated this peak with an artifact of the visibility window since it corresponds exactly to the fifth harmonic of the sidereal day (frequency at which observations were repeated). An alternative hypothesis (less favored) suggests it may be associated to the presence of a retrograde jet precession with a period of $\sim$170 days. We phase-folded the six individual data sets at P_r but the folded light curves do not appear aligned in phase.

4.3. Discussion

The X-ray and IR orbital modulations were clearly discovered in the 1970s, while a modulation of the radio emission was suspected at the orbital period in the 1980s during the observation of a mini flare of Cyg X-3 (Molnar et al. 1984). This hypothesis was later discarded looking at long-term radio observations with the Greenbank Interferometer at 2.25 and 8.3 GHz and the Ryle Telescope at 15 GHz. The lack of radio orbital modulation suggested that the bulk of the radio emission originates from a region outside the dense wind of the companion star causing the X-ray and IR scattering (Hjalmarsdotter et al. 2004), or that the radio emission originating relatively close to the jet base is completely free–free absorbed in the strong wind of the donor (Szostek & Zdziarski 2007). A recent analysis of the power spectrum associated with the 15 GHz data obtained with the Ryle Telescope and AMI over 22 yr has revealed a radio orbital modulation at the orbital period (Zdziarski et al. 2018). The modulation varies in amplitude (from 2.5% to 10%) and phase based on the X-ray spectral state and radio flux level of Cyg X-3.

We investigated the radio orbital modulation during specific episodes of Cyg X-3: the giant and mini radio flares. Observations of giant radio flares offer a unique opportunity to investigate the accretion/ejection link under extreme conditions. During such intense emission episodes, large-scale radio jets have been observed with interferometry. VLBA observations performed during the 2001 giant flare showed the expansion of a sequence of individual knots with an initial diameters of 8 mas (Miller-Jones et al. 2004). The jet precession was found to be over $\sim$5 days, significantly lower than during the 1997 flare where the precession period obtained was over 60 days (Mioduszewski et al. 2001). During the decaying emission of the 2017 giant flare, Medicina detected enhanced flux densities that seem to correspond to the orbital phase $\phi \sim 0.5$. This suggests that the emission from the base of the jet might be modulated at the orbital period. This could arise most likely from free–free absorption by thermal electrons from the wind of the Wolf–Rayet companion. Another scenario would be to assume that there are several jet components that compose the total flare, some of which are launched at the decaying phase of the major flare that could then be susceptible to wind absorption.

A recent VLBI observation of Cyg X-3 during a mini-flare indicated the presence of two peaks separated by $\sim$4.8 hr. The emission size associated to the flare was found to increase from 0.6 to 0.9 mas (radius) in a few hours (Egron et al. 2017), corresponding to $\sim 10^{14}$ cm for a distance of 7.4 kpc. We note that the light can cross this size in $\sim$1 hr, a value compatible with the peak width of the associated light curve shown in Figure 2. Thus, our combination of simultaneous timing and imaging through VLBI observations provides consistent results.

We therefore investigated additional mini-flare observations in order to search for evidence of the radio orbital modulation in Cyg X-3. In principle, the modulation of the radio emission should be more pronounced during mini-flares, which correspond to the emission of compact jets closer to the core than transient jets observed during giant flares. Indeed, we expect a higher density of radio-absorbing thermal electrons in this region (from the stellar wind of the companion star and/or from the jet itself) providing a higher opacity and then a stronger orbital modulation. We phase-folded the light curves

associated with the mini-flares at the X-ray orbital period using the most recent X-ray ephemeris (Bhargava et al. 2017). The 2016 mini-flare is found to be shifted with respect to the other mini-flares ($\phi \sim 0.5$ with respect to $\phi \sim 0$, respectively). The phase shift is most likely attributed to a different location of the radio-emitting region along the jet (Molnar et al. 1988; Newell et al. 1998; Egron et al. 2017).

The radio orbital modulation could be due to the free–free absorption in the stellar wind of the donor. In this case the minimum flux would be expected at $\phi = 0$, which corresponds to the longest line of sight. However, due to the large amplitude modulation in the light curve, it is difficult to account for such a strong absorption at jet distances much higher than the binary separation. Therefore at least part of the orbital flux modulation could also be attributed to variable/anisotropic shocks in the jet rather than a smooth wind attenuation alone. Note that Miller-Jones et al. (2009) arrived at the conclusion that synchrotron self-absorption and free–free absorption by entrained thermal material play a larger role in determining the opacity effects than absorption in the stellar wind of the Wolf–Rayet companion. Also Fender et al. (1997a; based on decreasing opacity of subsequent flares) and Koljonen et al. (2018; based on radio spectrum) arrived at the conclusion that the data support thermal plasma mixed with the synchrotron emitting particles, which likely means that the wind material is entrained in the jet rather than producing an absorbing screen.

Since the location of the radio emission along the jet can vary, timing correction for the motion and the variable location of the emitting region in different flaring episodes at different epochs would be required to correct for the delay. Moreover, jet proper motion as well as jet precession (Dubus et al. 2010; Zdziarski et al. 2018) could also affect the phase shift. For example, a jet ranging 10^{14} cm hr^{-1} during an observation (as those observed in 1985 and 1995) could provide an additional light-curve phase smearing effect. Better knowledge of the jet geometry, its motion, and the absorbing medium would be required to constrain precise time delays and fix related phase corrections. In any case, the observation of orbital modulation is still possible for the relevant height range, since the corresponding phase smearing during a mini-flare event is relatively low even in the unlikely "worst case" of a jet observed during superior/inferior conjunctions (for which timing corrections are at their maximum).

Since the jet extends to distances much larger than the orbital separation, it is also possible that while the compact object is exactly behind the donor, the radio-emitting region in the bent jet is exactly in front of the donor. In this configuration, the minimum radio flux is at $\phi = 0.5$. Interestingly enough, the 2016 mini-flare emission is found to be closer to the compact object (with respect to the 1985 and 1995 mini-flares), and the flux minimum corresponds to $\phi \sim 0.1$. Instead, the bulk of the radio emission associated with the other mini-flares is located further in the jet and the corresponding flux minimum is shifted by $\sim$0.5. This is consistent with a bent jet, as shown by Dubus et al. (2010) and clearly seen by the spatially resolved radio observations. The precession effects are expected to be stronger at a higher distance along the jet.

Zdziarski et al. (2018) studied the radio orbital modulation based on the X-ray spectral states and radio flux density. The modulation amplitude is found to be higher at low radio fluxes. Clear shifts of the phase of the modulation were observed in the soft, intermediate, and hard states, with a significant dependence on the flux density. The phase of the modulation minimum is found to increase with the increasing radio flux. It can be explained by the distance of the location of the bulk of radio emission increasing with the increasing flux and the jet being inclined with respect to the orbital axis. Interestingly enough, the peak of the radio orbital modulation associated with the data in the highest soft state considered by Zdziarski et al. (2018) is found at $\phi \sim 0.7$, which is also shifted with respect to the other states ($\phi \sim 0$), and consistent with our results.

The peculiarity of the 2016 mini-flare episode could hypothetically reside in the fact that it is seen during the hypersoft X-ray state, as clearly observed during the daily monitoring in X-rays with Swift/BAT (15–50 keV) and MAXI (2–10 keV), and in radio with SMA (220–230 GHz), AMI/LA (15 GHz), and RATAN (4–11 GHz) (Egron et al. 2017; Trushkin et al. 2017; Koljonen et al. 2018). The mini-flare was detected quasi-simultaneously to a hard X-ray mini-flare and an enhanced gamma-ray emission, a few weeks before the giant flare (Egron et al. 2017). Instead, the mini-flares in 1994, 1995, and 2002 did not occur in the hypersoft X-ray states, as shown by the radio/X-ray correlation studied by Zdziarski et al. (2016) using RXTE/ASM (1.3–12.2 keV), MAXI, Swift/BAT, CGRO/BATSE (20–100 keV), and Ryle/AMI (15 GHz). Unfortunately, we do not have information about the X-ray spectral states corresponding to the 1983 and 1985 mini-flares.

During the hypersoft state, the hard X-ray and radio flux densities reach their minima (the jet production is highly diminished or nearly turned off (1–30 mJy)) on a similar timescale, while the soft X-ray emission is at its maximum (McCollough et al. 1999). The conditions leading to the formation of the mini-flare during this particular state are likely different from the other ones. In particular, the compact jet appears to be closer to the compact object (Egron et al. 2017).

Fender et al. (1997a) suggest that during the radio quenched state (hypersoft X-ray state), the increase of the wind mass-loss rate from the WR star results in an increasing thermal electron density in the region of the compact object, at the location of the base of the jet. This would cause the disappearance of the jet although the exact mechanism remains unclear. Koljonen et al. (2018) propose a scenario to explain the spectral and timing properties of the multiwavelength observations, and favor the interpretation of changes in the accretion flow instead of changes in the stellar wind structure to explain the accretion state change to/from the hypersoft state. They attribute the residual radio emission (1–30 mJy) to the wind–wind interaction of the binary and not to the jet. Cao & Zdziarski (2020) suggest that during the hard to soft X-ray transition, the thin accretion disk extends to the innermost stable circular orbit and replaces the hot accretion flow. This quenches the generation of the internal magnetic field and causes the magnetic field to quickly diffuse away in the accretion disk, which explains the disappearance of the jets. In this scenario, the subsequent formation of the powerful jets visible during the major and giant radio flares is triggered at a large accretion rate due to the appearance of magnetic outflows above the thin accretion disk, which are able to efficiently advect the strong outer field from the Wolf–Rayet.

Also, due to the short orbital distance, the compact object is orbiting the Wolf–Rayet star inside the strong wind, which causes interaction between several components—e.g., the jet

hitting the wind modulates shocks that dissipate energy effectively. Despite the fast wind speed of the Wolf–Rayet companion, clumps in the wind (de la Cita et al. 2017) could also contribute to a variable and efficient accretion process in addition to a different density in the wind.

5. Conclusions

Cyg X-3 observations carried out with Medicina at 8.5, 18.6, and 24.1 GHz, parallel to the MRO at 37 GHz, allowed us to study the evolution of the spectral index along the whole duration of the 2017 giant flare. We confirmed a spectral steepening at the time of the peak maximum of the flare, as observed when previous giant flares had occurred. We highlighted different spectral index variations during the fading of the flare associated with fast changes of the radio emission. A first attempt in the study of the orbital modulation seems to demonstrate that the enhanced radio emissions during the decaying flare might correspond to the orbital phase $\phi \sim 0.5$. This suggests that the base of the jet could be modulated at the orbital period most likely from free–free absorption by thermal electrons from the wind of the Wolf–Rayet companion.

The peak separation of $\sim$4.8 hr during different single observations most likely indicates an effect of the modulation of the radio emission at the orbital period of the system. Therefore, we systematically searched for radio orbital modulation during mini-flares of Cyg X-3, associated with compact radio emission. Using the X-ray ephemeris, we found that all the folded light curves appear to be aligned in phase, peaking at $\phi \sim 0$, except for the 2016 light curve, which is shifted by $\sim$0.5 with respect to the other ones. The phase shift is likely attributed to a different location of the bulk of the radio emission along the bent jet during the different mini-flare episodes. Time delays arising from jet emission at altitudes $\geqslant 10^{14}$ cm can provide significant phase shift >0.2 (the actual value depending on the jet position and inclination with respect to the observer's line of sight). The precise location of the radio-emitting regions with respect to the accretion disk and the observer is uncertain, even though VLBI observations are shedding some light on the actual dynamic geometry (altitude, extension, line-of-sight inclinations, precession, etc.) during the different jet emission episodes. The shift might also be explained by a particular configuration of the system when the compact object is exactly behind the donor, the radio-emitting region in the inclined jet can be exactly in front of the donor. In this case, the minimum radio flux is at $\phi \sim 0.5$. In both hypotheses, the phase shift is explained by the large and variable extension of the jets with respect to the orbital separation and radius of the donor. The observed large depths in the folded light curves place doubt on the possibility that the orbital modulation could be fully attributed to free–free absorption in the stellar wind if the emission is occurring at large distances from the binary system. A contribution of variable/anisotropic shocks in the jet could explain at least part of the modulation.

Our timing results might suggest that the studied mini-flares occurred during different accretion states and/or different emission geometries. Furthermore, the different peak widths and light-curve shapes observed during mini-flare episodes could be explained as phase smearing effects related to jet proper motion and precession. In extreme cases this could also prevent orbital period detection, if for example the proper motion along the line of sight exceeded 5×10^{14} cm hr^{-1}.

Additional observations of mini-flares in radio, X-rays, and gamma rays during different states of the source will help to shed light on the phase shift observed in our present data sets. In particular, further VLBI observations are needed to better constrain the emission geometry also required for coherent timing analysis.

We thank the referee for constructive suggestions, which improved the discussion of the paper. Based on observations with the Medicina telescope operated by INAF—Istituto di Radioastronomia. We thank A. Zanichelli for promptly scheduling the Medicina observations. The Sardinia Radio Telescope is funded by the Department of University and Research (MIUR), the Italian Space Agency (ASI), and the Autonomous Region of Sardinia (RAS), and is operated as a National Facility by the National Institute for Astrophysics (INAF). The Torun radio telescope is operated by Torun Centre for Astronomy of Nicolaus Copernicus University in Torun (Poland) and supported by the PolishMinistry of Science andHigher Education SpUBgrant. S.C. acknowledges the financial support from the UnivEarthS Labex program of Sorbonne Paris Cité (ANR-10-LABX-0023 and ANR-11-IDEX-0005-02). V.G. is supported through the Margarethe von Wrangell fellowship by the European Social Fund and the Ministry of Science, Research and the Arts Baden-Württemberg. J.R. ackowledges partial funding from the French space agency (CNES).

ORCID iDs

Elise Egron https://orcid.org/0000-0002-1532-4142
Alberto Pellizzoni https://orcid.org/0000-0002-4590-0040
Simona Righini https://orcid.org/0000-0001-7332-5138
Marcello Giroletti https://orcid.org/0000-0002-8657-8852
Karri Koljonen https://orcid.org/0000-0002-9677-1533
Katja Pottschmidt https://orcid.org/0000-0002-4656-6881
Jessica Lobina https://orcid.org/0000-0001-7738-2244
Maura Pilia https://orcid.org/0000-0001-7397-8091
Joern Wilms https://orcid.org/0000-0003-2065-5410
Victoria Grinberg https://orcid.org/0000-0003-2538-0188
Sara Loru https://orcid.org/0000-0001-5126-1719
Jérome Rodriguez https://orcid.org/0000-0002-4151-4468
A. Lähteenmäki https://orcid.org/0000-0002-0393-0647
M. Tornikoski https://orcid.org/0000-0003-1249-6026

References

Atoyan, A. M., & Aharonian, F. A. 1999, MNRAS, 302, 253
Becklin, E. E., Neugebauer, G., Hawkins, F. J., et al. 1973, Natur, 245, 302
Bhargava, Y., Rao, A. R., Singh, K. P., et al. 2017, ApJ, 849, 141
Brocksopp, C., Fender, R. P., & Pooley, G. G. 2002, MNRAS, 336, 699
Canizares, C. R., McClintock, J. E., Clark, G. W., et al. 1973, NPhS, 241, 28
Cao, X., & Zdziarski, A. A. 2020, MNRAS, 492, 223
Corbel, S., Dubus, G., Tomsick, J. A., et al. 2012, MNRAS, 421, 2947
Davidsen, A., & Ostriker, J. P. 1974, ApJ, 189, 331
de la Cita, V. M., del Palacio, S., Bosch-Ramon, V., et al. 2017, A&A, 604, A39
Deller, A. T., Brisken, W. F., Phillips, C. J., et al. 2011, PASP, 123, 275
Dubus, G., Cerutti, B., & Henri, G. 2010, MNRAS, 404, L55
Egron, E., Pellizzoni, A., Giroletti, M., et al. 2017, MNRAS, 471, 2703
Fender, R. P., Bell Burnell, S. J., Waltman, E. B., et al. 1997a, MNRAS, 288, 849
Fender, R. P., Belloni, T. M., & Gallo, E. 2004, MNRAS, 355, 1105
Fender, R. P., Brocksopp, C., & Pooley, G. G. 1997b, IAUC, 6544, 2
Fermi LAT Collaboration, Abdo, A. A., Ackermann, M., et al. 2009, Sci, 326, 1512

Giacconi, R., Gorenstein, P., Gursky, H., & Waters, J. R. 1967, ApJL, 148, L119
Guo, F., Li, H., Daughton, W., & Liu, Y.-H. 2014, PhRvL, 113, 155005
Hjalmarsdotter, L., Hakala, P. J., Vilhu, O., et al. 2004, RMxAC, 20, 216
Hjalmarsdotter, L., Zdziarski, A. A., Larsson, S., et al. 2008, MNRAS, 384, 278
Hjalmarsdotter, L., Zdziarski, A. A., Szostek, A., & Hannikainen, D. C. 2009, MNRAS, 392, 251
Hjellming, R. M., & Johnston, K. J. 1988, ApJ, 328, 600
Kitamoto, S., Hirano, A., Kawashima, K., et al. 1995, PASJ, 47, 233
Kitamoto, S., Miyamoto, S., Matsui, W., & Inoue, H. 1987, PASJ, 39, 259
Koljonen, K. I. I., Hannikainen, D. C., McCollough, M. L., Pooley, G. G., & Trushkin, S. A. 2010, MNRAS, 406, 307
Koljonen, K. I. I., Maccarone, T., McCollough, M. L., et al. 2018, A&A, 612, A27
Koljonen, K. I. I., & Maccarone, T. J. 2018, MNRAS, 474, 572
Lindfors, E. J., Türler, M., Hannikainen, D. C., et al. 2007, A&A, 473, 923
Martí, J., Paredes, J. M., & Peracaula, M. 2001, A&A, 375, 476
McCollough, M. L., Corrales, L., & Dunham, M. M. 2016, ApJL, 830, L36
McCollough, M. L., Robinson, C. R., Zhang, S. N., et al. 1999, ApJ, 517, 951
Miller-Jones, J. C. A., Blundell, K. M., Rupen, M. P., et al. 2004, ApJ, 600, 368
Miller-Jones, J. C. A., Rupen, M. P., Türler, M., et al. 2009, MNRAS, 394, 309
Mioduszewski, A. J., Rupen, M. P., Hjellming, R. M., Pooley, G. G., & Waltman, E. B. 2001, ApJ, 553, 766
Molina, E., del Palacio, S., & Bosch-Ramon, V. 2019, A&A, 629, A129
Molnar, L. A., Reid, M. J., & Grindlay, J. E. 1984, Natur, 310, 662
Molnar, L. A., Reid, M. J., & Grindlay, J. E. 1988, ApJ, 331, 494
Newell, S. J., Garrett, M. A., & Spencer, R. E. 1998, MNRAS, 293, L17
Ott, M., Witzel, A., Quirrenbach, A., et al. 1994, A&A, 284, 331
Parsignault, D. R., Gursky, H., Kellogg, E. M., et al. 1972, NPhS, 239, 123
Pooley, G. G., Fender, R. P., & Brocksopp, C. 1999, MNRAS, 302, L1
Singh, N. S., Naik, S., Paul, B., et al. 2002, A&A, 392, 161
Sironi, L., Giannios, D., & Petropoulou, M. 2016, MNRAS, 462, 48
Sironi, L., & Spitkovsky, A. 2014, ApJL, 783, L21
Szostek, A., & Zdziarski, A. A. 2007, MNRAS, 375, 793
Szostek, A., Zdziarski, A. A., & McCollough, M. L. 2008, MNRAS, 388, 1001
Tavani, M., Bulgarelli, A., Piano, G., et al. 2009, Natur, 462, 620
Teräesranta, H., Tornikoski, M., Mujunen, A., et al. 1998, A&AS, 132, 305
Trushkin, S., McCollough, M., Nizhelskij, N., & Tsybulev, P. 2017, Galax, 5, 86
Tudose, V., Fender, R. P., Garrett, M. A., et al. 2007, MNRAS, 375, L11
van der Klis, M., & Bonnet-Bidaud, J. M. 1981, A&A, 95, L5
van der Laan, H. 1966, Natur, 211, 1131
van Kerkwijk, M. H., Charles, P. A., Geballe, T. R., et al. 1992, Natur, 355, 703
van Kerkwijk, M. H., Geballe, T. R., King, D. L., van der Klis, M., & van Paradijs, J. 1996, A&A, 314, 521
Waltman, E. B., Fiedler, R. L., Johnston, K. J., & Ghigo, F. D. 1994, AJ, 108, 179
Waltman, E. B., Foster, R. S., Pooley, G. G., Fender, R. P., & Ghigo, F. D. 1996, AJ, 112, 2690
Waltman, E. B., Ghigo, F. D., Johnston, K. J., et al. 1995, AJ, 110, 290
Zdziarski, A. A. 2012, MNRAS, 422, 1750
Zdziarski, A. A., Maitra, C., Frankowski, A., Skinner, G. K., & Misra, R. 2012, MNRAS, 426, 1031
Zdziarski, A. A., Malyshev, D., Dubus, G., et al. 2018, MNRAS, 479, 4399
Zdziarski, A. A., Mikołajewska, J., & Belczyński, K. 2013, MNRAS, 429, L104
Zdziarski, A. A., Segreto, A., & Pooley, G. G. 2016, MNRAS, 456, 775